Sphingolipid metabolism governs Purkinje cell patterned degeneration in *Atxn1[82Q]/+* mice

François G. C. Blot[a,1], Wilhelmina H. J. J. Krijnen[a], Sandra Den Hoedt[b], Catarina Osório[a], Joshua J. White[a], Monique T. Mulder[b], and Martijn Schonewille[a,1]

[a]Department of Neuroscience, Erasmus Medical Center, 3015 GE Rotterdam, The Netherlands; and [b]Department of Internal Medicine, Erasmus Medical Center, 3015 GE Rotterdam, The Netherlands

Edited by Tobias C. Walther, Harvard School of Public Health, Boston, MA, and accepted by Editorial Board Member Nancy Y. Ip July 19, 2021 (received for review August 11, 2020)

Patterned degeneration of Purkinje cells (PCs) can be observed in a wide range of neuropathologies, but mechanisms behind nonrandom cerebellar neurodegeneration remain unclear. Sphingolipid metabolism dyshomeostasis typically leads to PC neurodegeneration; hence, we questioned whether local sphingolipid balance underlies regional sensitivity to pathological insults. Here, we investigated the regional compartmentalization of sphingolipids and their related enzymes in the cerebellar cortex in healthy and pathological conditions. Analysis in wild-type animals revealed higher sphingosine kinase 1 (Sphk1) levels in the flocculonodular cerebellum, while sphingosine-1-phosphate (S1P) levels were higher in the anterior cerebellum. Next, we investigated a model for spinocerebellar ataxia type 1 (SCA1) driven by the transgenic expression of the expanded Ataxin 1 protein with 82 glutamine (82Q), exhibiting severe PC degeneration in the anterior cerebellum while the flocculonodular region is preserved. In *Atxn1[82Q]/+* mice, we found that levels of Sphk1 and Sphk2 were region-specific decreased and S1P levels increased, particularly in the anterior cerebellum. To determine if there is a causal link between sphingolipid levels and neurodegeneration, we deleted the *Sphk1* gene in *Atxn1[82Q]/+* mice. Analysis of *Atxn1[82Q]/+; Sphk1*$^{-/-}$ mice confirmed a neuroprotective effect, rescuing a subset of PCs in the anterior cerebellum, in domains reminiscent of the modules defined by AldolaseC expression. Finally, we showed that Sphk1 deletion acts on the ATXN1[82Q] protein expression and prevents PC degeneration. Taken together, our results demonstrate that there are regional differences in sphingolipid metabolism and that this metabolism is directly involved in PC degeneration in *Atxn1[82Q]/+* mice.

sphingolipid | Atxn[82Q] | Purkinje cell | S1P | AldolaseC

Purkinje cells (PCs) integrate all afferent sensorimotor information using their massive dendritic tree and form the exclusive output source of the cerebellar cortex. Based on the highly structured and repetitive organization of the cerebellar cortex, PCs are often regarded as a homogeneous population of neurons. However, for several decades anatomical and immunohistochemical studies have emphasized that different subtypes of PCs can be identified in the cerebellar cortex, including transverse zones (e.g., the anterior vs. flocculonodular cerebellum), parasagittal modules (e.g., AldolaseC [AldoC]-positive vs. AldoC-negative domains), and others (such as apex vs. sulcus or vermis vs. hemispheres) (reviewed in ref. 1). Regional differences in PC density (2), dendritic arborization (3), morphology of organelles (4), and axonal thickness (5) can be observed across the cerebellar cortex. The most commonly studied pattern is defined by AldoC (also known as ZebrinII) expression, which divides PC subtypes in parasagittal bands with distinct molecular footprints (6–9) and distinct electrophysiological intrinsic and synaptic properties (10–12), as well as input/output connectivity (13, 14). Cerebellar heterogeneity is also illustrated by the nonhomogeneous and nonrandom PC degeneration across the cerebellar cortex observed in a broad spectrum of cerebellar pathologies. These cerebellar pathologies, displayed by patients or rodent models, can result from genetic mutations, such as *leaner* (15), *Harlequin* (16), *sticky* (17), *Slc9a6*$^{-/-}$ (18), and *Cav2.1*$^{-/-}$ (19), as well as brain ischemia (20), viral infections (21), prion diseases (22), and alcohol abuse, such as alcohol-related cerebellar degeneration (23). As described by Sarna and Hawkes (24), not all patterned neurodegenerations are similar. Two main types of patterned degeneration have been observed: 1) pathologies in which the flocculonodular cerebellum is more resistant, leading to a clear separation regarding the progression of the neurodegeneration between anterior cerebellum and flocculonodular lobule, and 2) pathologies in which PC degeneration affects primarily AldoC-negative domains, leading to parasagittal compartmentalization of neurodegeneration. Thus far, mechanisms explaining the patterned neurodegeneration of PCs have not been revealed, although some cellular pathways have been investigated (25), or suggested, such as the metabolism of sphingolipids (24). Sphingolipids are essential bioactive sphingoid-based complex lipids that regulate physiological processes such as cell differentiation, neurogenesis,

Significance

Neuronal subtypes are differentially affected by neuropathologies. For example, Purkinje cells, the principal neurons of the cerebellum, can be divided in subpopulations based on their sensitivity to pathological insult. However, the molecular mechanisms explaining why, among seemingly identical neurons, some will degenerate while others survive remain unknown. Here, we analyzed, in a disease model of cerebellar neurodegeneration, the metabolism of sphingolipids, complex lipids involved in cell apoptosis, and found that specific sphingolipids accumulate in the cerebellar region primarily affected by neurodegeneration. Preventing this accumulation by disrupting sphingolipid metabolism via genetic mutation caused a neuroprotective effect on subpopulations of Purkinje cells. Thus, our data indicate that sphingolipid metabolism is involved in the predisposition of neuronal subtypes to neurodegeneration.

Author contributions: F.G.C.B. designed research; F.G.C.B. and W.H.J.J.K. performed research; F.G.C.B., W.H.J.J.K., S.D.H., C.O., and J.J.W. analyzed data; and F.G.C.B., S.D.H., C.O., J.J.W., M.T.M., and M.S. wrote the paper.

The authors declare no competing interest.

This article is a PNAS Direct Submission. T.C.W. is a guest editor invited by the Editorial Board.

[1]To whom correspondence may be addressed. Email: francois.blot@inserm.fr or m.schonewille@erasmusmc.nl.

This article contains supporting information online at https://www.pnas.org/lookup/suppl/doi:10.1073/pnas.2016969118/-/DCSupplemental.

Published September 3, 2021.

synaptic strengthening, and cell survival (26–29). Particularly, sphingosine-1-phosphate (S1P) is a potent bioactive modulator, acting intracellularly or in an autocrine/paracrine manner (30). S1P is the product of sphingosine (Sph) phosphorylation, which is catalyzed by sphingosine kinases (Sphks; Sphk1 and Sphk2) and can be reversed by dephosphorylation through sphingosine phosphate phosphatases (Sgpps; Sgpp1 and Sgpp2) or irreversibly degraded by S1P lyase (31). Both Sph and S1P are part of ceramide metabolism, known to be a central mediator in programmed cell death (32). The S1P/ceramide ratio, or rheostat, is decisive for cell fate in several tissues (33), and tight regional control has been correlated with local neuroprotective effects in structures of the central as well as peripheral nervous system (34, 35). PCs are known to be sensitive to sphingolipid levels, as decreasing ceramide and Sph levels by blocking the de novo ceramide synthesis pathway through the serine palmitoyltransferase inhibitor led to a decrease in survival rate of PCs in culture (36). Conversely, enrichment of culture media with ceramide, Sph, or dihydroceramide promoted PC survival. In vivo, PC degeneration was observed in mutant models targeting proteins involved in the sphingolipid pathway, such as ceramide synthase CerS1 (37), Acid Ceramidase 3 (38), and Saposin D (39, 40). Typically, all those mutants show either preferential degeneration of the anterior cerebellum or AldoC-negative PCs, patterns which could appear similar but remain clearly distinct after proper scrutinization. In mouse models of Niemann–Pick disease types A and C, featuring loss of function of acid ceramidase or Niemann–Pick C1 Protein, respectively, patterned PC degeneration was clearly described (41). Although most of these data indicate an antiapoptotic role of S1P in PCs, accumulation of long-chain bases Sph and S1P has also been reported as proapoptotic in vitro (42) and in vivo (43, 44), and restoring long-chain base levels rescued the neurodegenerative phenotype in the CerS1 mouse model (45). Altogether, this stresses the impact of sphingolipid homeostasis on PC fate. Therefore, we investigated the possible role of local sphingolipid metabolism on cerebellar patterned neurodegeneration. Here, we show that in adult wild-type mice, Sphk1 levels are higher in the flocculonodular region, while the levels of its product, S1P, are higher in the anterior region. We then investigated changes in sphingolipid levels in the *Atxn1[82Q]*/+ mice model of the spinocerebellar ataxia type 1 (SCA1) (46). The neurodegeneration observed in this model results from the expression and localization of the polyglutamine mutant protein in the nucleus (47). In *Atxn1[82Q]*/+ mice, degeneration primarily affects the anterior region, while the flocculonodular lobule remains spared over an extended course of the disease (46, 48–50). We found that this prevalence correlates with increased S1P levels and region-specific decreases in Sphk1 and Sphk2 expression levels compared to wild-type mice. To test the potential contribution of Sphk1 activity to neurodegeneration, we crossed *Atxn1[82Q]*/+ mice with *Sphk1* knockout mice (*Sphk1*$^{-/-}$). Whereas *Sphk1*$^{-/-}$ mice did not exhibit cerebellar defects or significant changes in S1P levels, the deletion of *Sphk1* in *Atxn1[82Q]*/+ mice resulted in a neuroprotective effect on a subset of PCs. The deletion of Sphk1 affects the expression of ATXN1[82Q] protein and reduces somatic PC atrophy in defined domains reminiscent of AldoC-positive PC modules. Taken together, we show that sphingolipid metabolism can impact the expression of misfolded proteins and, thereby, play a major role in patterned PC degeneration.

Results

Sphk1, Unlike Sphk2, Exhibit Region-Dependent Expression in the Adult Cerebellum. Sphk1 and Sphk2 are two protein isoforms responsible for the phosphorylation of Sph to produce S1P (Fig. 1*A*). Previous work showed a nonuniform expression of Sphk1 in cerebellar PCs (51). To determine if Sphk1 and Sphk2 levels are region-specific, we quantified the relative protein levels in the anterior and the flocculonodular fraction in wild-type mice (littermate of the *Atxn1[82Q]*/+ mice). For both juveniles and adults, the Sphk1 expression levels in the flocculonodular fraction were significantly higher than in the anterior fraction (juvenile: $P < 0.05$ and adult: $P < 0.005$) (Fig. 1 *B* and *C* and *SI Appendix*, Fig. S1). In contrast, the expression levels of the isoenzyme Sphk2 were not different between both fractions (juvenile mice $P = 0.168$, adult mice $P = 1.00$). When comparing juvenile and adult mice, Sphk1 expression levels did not change (anterior: $P = 1.00$; flocculonodular: $P = 0.584$), while Sphk2 expression levels increased from juvenile to adult (anterior: $P < 0.001$; flocculonodular: $P < 0.001$). Thus, only Sphk1 shows signs of cerebellar region–specific differences in expression, with the higher levels in the flocculonodular fraction being consistent across ages across ages.

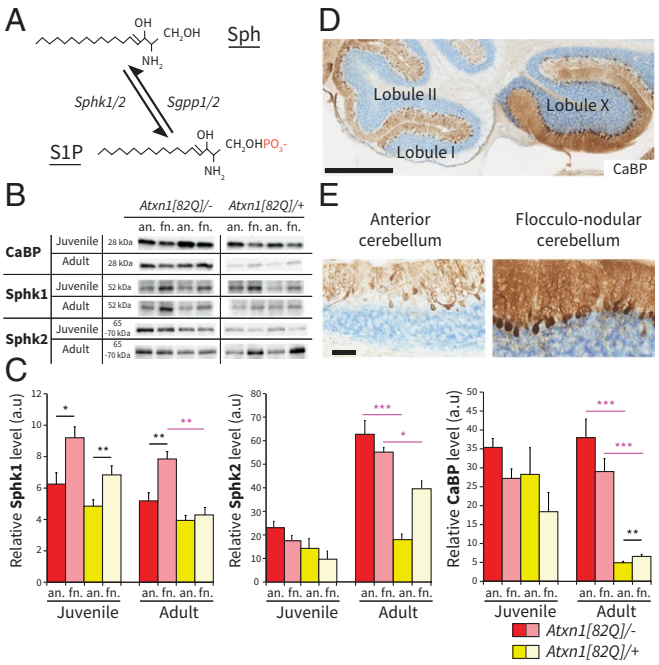

Fig. 1. Sphk1 and Sphk2 expressions are region dependent in wild-type and *Atxn1[82Q]*/+ mice. (*A*) Schematic representation of Sph phosphorylation in S1P through the addition of a phosphate group (red) by kinases Sphk1/2 and the reverse reaction driven by phosphatases Sgpp1/2. (*B*) Western blotting images of CaBP, Sphk1, and Sphk2 expression levels in anterior and flocculonodular regions of *Atxn1[82Q]*/+ and wild-type littermates *Atxn1[82Q]*/—. (*C*) Bar plot of western blotting protein quantification for CaBP ($n = 5$ per group), Sphk1 ($n = 5$ per group), and Sphk2 ($n = 4$ per group) expression levels. (*D*) Immunohistochemistry for CaBP protein in a P140 *Atxn1[82Q]*/+ sagittal cerebellar section. (Scale bar: 500 μm.) (*E*) High magnification of the cerebellar cortex in anterior and flocculonodular regions. Data are shown as mean ± SEM. Juvenile indicates P21 to P23, and adult indicates P143 to P153. (Scale bar: 50 μm.) Statistical analyses for western blot protein quantification were performed using Levene's test for equality followed by Student's *t* test following "paired" to compare anterior vs. flocculonodular fractions (black asterisks) and "unpaired" to compare *Atxn1[82Q]*/– vs. *Atxn1[82Q]*/+ (purple asterisks), with Bonferroni correction for multiple comparisons. an., anterior; fn., flocculonodular; a.u., arbitrary unit. *$P < 0.05$; **$P < 0.005$; ***$P < 0.001$.

Region-Specific Changes in Sphk1 and Sphk2 Expression Levels in *Atxn1[82Q]*/+ Mice. The *Atxn1[82Q]*/+ mouse (52) is a model of SCA1 driven by the overexpression of the expanded Ataxin1 (ATXN1) protein with 82 glutamine (82Q) repeats under the control of the PC-specific Pcp2 promoter. This model has been shown to have relatively normal cerebellar development up to

postnatal day 25 (P25), with no apparent signs of morphological changes in PCs (46). The neuropathology is apparent from 5 to 6 wk and characterized by PC atrophy, disorganization of the PC monolayer with ectopic PCs, and reduction of calbindin (CaBP) expression. One feature of the *Atxn1[82Q]*/+ mouse model, also identified in the human pathology, is that the neurodegenerative process unfolds more rapidly in the anterior region, leaving the flocculonodular region spared (46, 50) (Fig. 1 *D* and *E*). The differential degeneration in adult mice was confirmed by western blot quantification that showed a decrease of CaBP expression levels in both fractions of the mutant compared with the wild type (*Atxn1[82Q]*/– vs. *Atxn1[82Q]*/+ anterior: $P < 0.001$; flocculonodular: $P < 0.001$) but with higher expression levels in the flocculonodular fraction compared with the anterior fraction in the *Atxn1[82Q]*/+ mice ($P < 0.005$) (Fig. 1 *C*–*E* and *SI Appendix*, Fig. S1). Correlation between sphingolipid metabolism and spinocerebellar ataxia has been described previously (53) but has been largely focused on ceramide, sphingomyelin, and ganglioside metabolism, instead of S1P synthesis. To investigate a potential involvement of this part of the pathway in spinocerebellar ataxia, we measured Sphk1 and Sphk2 expression levels in cerebellar fractions of *Atxn1[82Q]*/+ mice. In juvenile *Atxn1[82Q]*/+ mice, Sphk1 expression levels did not significantly differ from wild-type mice (all $P > 0.05$), replicating the difference between anterior and flocculonodular fractions ($P < 0.005$) (Fig. 1 *B* and *C* and *SI Appendix*, Fig. S1). In the adult *Atxn1[82Q]*/+ mice, unlike in the wild-type mice, there was no significant difference in the expression of Sphk1 between the anterior and flocculonodular fractions ($P = 1.00$). The loss of region-specific difference was primarily caused by a robust decrease of Sphk1 in the flocculonodular fraction (*Atxn1[82Q]*/– vs. *Atxn1[82Q]*/+; $P < 0.005$), as there is no significant decrease in the anterior fraction (*Atxn1[82Q]*/– vs. *Atxn1[82Q]*/+; $P = 0.295$). Conversely, in adult *Atxn1[82Q]*/+ mice, the Sphk2 expression levels were more than halved in the anterior fraction compared with wild-type mice (*Atxn1[82Q]*/– vs. *Atxn1[82Q]*/+; $P < 0.001$), with a smaller decrease in the flocculonodular fractions ($P < 0.05$) (Fig. 1 *D* and *E* and *SI Appendix*, Fig. S1). Taken together, these data show that cerebellar neurodegeneration following the expression of the Atxn1[82Q] transgene in PCs correlates with a reduction of the expression levels of both Sphk1 and Sphk2, but the magnitude of the changes is directly dependent on the cerebellar region.

S1P Levels Differ between Fractions in Wild-Type Mice. The differential Sphk1 expression levels between fractions in wild-type mice suggest a tight regulation of sphingolipids levels in distinct regions of the cerebellum in healthy conditions. We used high-performance liquid chromatography with tandem mass spectrometry (HPLC-MS/MS) to measure the relative levels of S1P, Sph, ceramides, and sphingomyelins in both the anterior and the flocculonodular fractions. All sphingolipids are composed of Sph, an 18-carbon chain with one double bound (d18:1), which for ceramides and sphingomyelins, is associated with a fatty acid of variable length (d18:1/[fatty acid carbon number]:[fatty acid double bonds]). We found that S1P(d18:1) levels were significantly higher in the anterior fraction than the flocculonodular fraction ($P < 0.001$) (Fig. 2 *A* and *B*) in wild-type adult mice. These differential levels emerged later in development as no significant differences were observed between fractions in juvenile mice ($P = 0.496$). Despite a trend in adult mice, Sph(d18:1) levels were not significantly different between fractions at both ages after correction for multiple comparisons. When we examined the levels of ceramides and sphingomyelin, other prominent lipids in the cascade, we found no significant differences between anterior and flocculonodular fractions, neither in juvenile nor in adult wild-type mice (all $P > 0.05$) (Fig. 2*A* and *SI Appendix*, Fig. S2*A*). These data, together with the protein expression, highlight

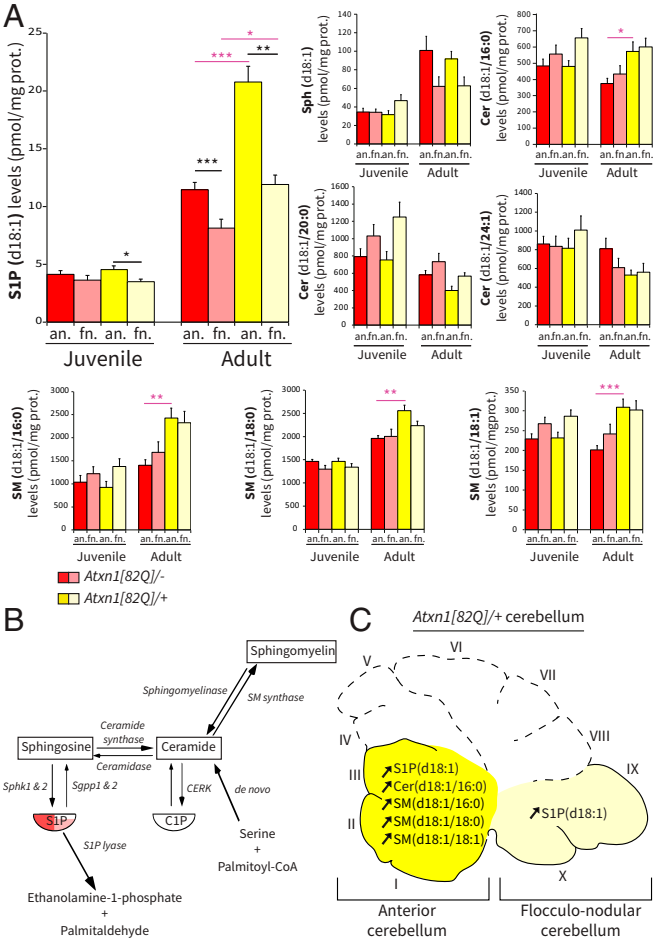

Fig. 2. S1P(d18:1) levels are different between fractions in adult wild-type *Atxn1[82Q]*/–, and in *Atxn1[82Q]*/+ mice, S1P, ceramide, and sphingomyelin are increased in the anterior cerebellum. (*A*) Bar plot of HPLC-MS/MS quantification of selected sphingolipid levels in wild-type *Atxn1[82Q]*/– (FVB/N) and mutant *Atxn1[82Q]*/+ mice. (*B*) Schematic of the sphingolipid metabolic pathway with representation of level differences between anterior (red) and flocculonodular (pink) fractions. (*C*) Schematic of the sagittal view of the *Atxn1[82Q]*/+ cerebellum with identification of the fractions and annotation of the sphingolipid changes measured in the mutant in independent fractions. Data are expressed as mean ± SEM ($n = 10$ per group); the unit is picomoles per milligram of protein. Juvenile indicates P21 to P23, and adult indicates P143 to P153. Statistical analyses for LC-MS/MS lipid quantification were performed using Levene's test for equality followed by Student's *t* test paired to compare anterior vs. flocculonodular fractions (black asterisks) and unpaired to compare *Atxn1[82Q]*/– vs. *Atxn1[82Q]*/+ (purple asterisks), with Bonferroni correction for multiple comparisons. an., anterior; fn., flocculonodular; Cer/CER, ceramide; CERK, ceramide kinase; SM, sphingomyelin. *$P < 0.05$; **$P < 0.005$; ***$P < 0.001$.

the tight and specific region-dependent control on S1P levels in wild-type animals (Fig. 2*B*).

Increased Levels of S1P in the Anterior Cerebellum of Adult *Atxn1[82Q]*/+ Mice. Given that cerebellar regions exhibit differential vulnerability to neurodegeneration, we then investigated regional sphingolipid levels in the *Atxn1[82Q]*/+ mouse. In adult mice, we observed a robust increase of S1P(d18:1) levels in the anterior cerebellar fraction of *Atxn1[82Q]*/+ adult mice when compared with wild-type animals (*Atxn1[82Q]*/–: 11.5 ± 1.27 pmol/mg; *Atxn1[82Q]*/+: 20.76 ± 2.74 pmol/mg; *Atxn1[82Q]*/– vs. *Atxn1[82Q]*/+; $P < 0.001$) (Fig. 2 *A* and *C*). A significant

but smaller increase of S1P(d18:1) levels was also observed in the flocculonodular fraction of the mutant (*Atxn1[82Q]*/–: 8.16 ± 1.46 pmol/mg; *Atxn1[82Q]*/+: 11.90 ± 1.68 pmol/mg; *Atxn1[82Q]*/– vs. *Atxn1[82Q]*/+; $P < 0.05$). To determine whether the increases of S1P represent an overall increase of sphingolipid metabolism, we quantified several ceramides and sphingomyelins. Strikingly, all significant differences observed between wild-type and mutant mice were restricted to the anterior fraction, as Cer(d18:1/16:0) ($P < 0.05$), SM(d18:1/16:0) ($P < 0.005$), SM(d18:1/18:0) ($P < 0.005$), and SM(d18:1/18:1) ($P < 0.001$) levels increased compared with wild-type mice (Fig. 2 *A* and *C*). The variations observed in sphingolipids suggest a complex mechanism with down- and up-regulation of different enzymes and isoenzymes in the pathway. Despite changes in both upstream and downstream metabolites, Sph(d18:1) levels were unaffected, with no overall changes between the wild type and mutant (anterior: *Atxn1[82Q]*/– vs. *Atxn1[82Q]*/+; $P = 1.00$; flocculonodular: *Atxn1[82Q]*/– vs. *Atxn1[82Q]*/+; $P = 1.00$). In contrast to the anterior fraction, none of the ceramide or sphingomyelin levels were significantly changed in the flocculonodular fraction of mutant *Atxn1[82Q]*/+ mice (all $P > 0.05$) (Fig. 2*A* and *SI Appendix*, Fig. S2). Moreover, in juvenile *Atxn1[82Q]*/+ mice that lack signs of neurodegeneration, all sphingolipid levels did not differ significantly from wild-type mice in both fractions (all $P > 0.05$) (Fig. 2*A* and *SI Appendix*, Fig. S2*A*). We show that sphingolipid levels change with the temporal and spatial progression of the neurodegeneration and that the increase in S1P is most prominent in the anterior region, which is most affected by the pathology. These results demonstrate a clear correlation between sphingolipid levels and neurodegeneration.

Sphk1 Deletion Has Marginal Effects on Sphingolipid Levels and Cerebellum-Dependent Behavior. To further investigate the role of S1P synthesis in PCs, we evaluated the consequences of *Sphk1* knockout on cerebellar sphingolipid levels, development, and function. The deletion of the Sphk1 protein in *Sphk1*$^{-/-}$ mice was confirmed in both cerebellar fractions (*SI Appendix*, Fig. S3*A*). Sphks convert Sph into S1P; thus, the deletion of Sphk1 could have both a direct effect on S1P levels and/or indirect repercussions upstream in the pathway. The deletion of Sphk1 had no measurable effect on the levels of S1P(d18:1), Sph(d18:1), or any other sphingolipid levels (Fig. 3 *A* and *C* and *SI Appendix*, Fig. S2*B*) (all $P > 0.05$). This argued against a general decrement of the pathway. We also observed that in the C57BL/6-J wild-type mice, several ceramide levels were significantly higher in the flocculonodular fraction (Fig. 3*A*). *Sphk1*$^{-/-}$ mice were previously described to have no major neurological impairments (54); however, the cerebellum and cerebellar functions have not been explicitly evaluated. Immunostaining for CaBP revealed no apparent developmental defects in lobulation, laminar organization, neuronal migration, or any degenerative processes, such as PC torpedoes or PC atrophy at P140 (*SI Appendix*, Fig. S3*B*). To further investigate the effect of deleting Sphk1 on cerebellar development and function, we subjected *Sphk1*$^{-/-}$ and wild-type *Sphk1*$^{+/+}$ littermate mice to adaptive locomotor and balance-related tasks. There was no significant difference between wild-type and mutant mice subjected to the balance beam task in the relative number of slips on the 12-mm (thick) or 6-mm (thin) beam at 6, 12, and 18 wk or in the time to cross the thick or thin beam at 6, 12, and 18 wk (*SI Appendix*, Fig. S3*C*). In addition, locomotion behavior of these mice was examined longitudinally using the Erasmus Ladder (*SI Appendix*, Fig. S3*D*). In the training weeks, a significant increase of the ratio of long steps vs. short steps was found over time for both genotypes ($P < 0.001$), and no differences were observed between *Sphk1*$^{+/+}$ and *Sphk1*$^{-/-}$ ($P = 0.208$). Mouse performance in the following weeks did not improve over time ($P = 0.087$) and did not differ between genotypes ($P = 0.460$). Together, these data indicate that deletion of *Sphk1* shows marginal changes in measured sphingolipid levels without any effects on cerebellum-dependent behavior.

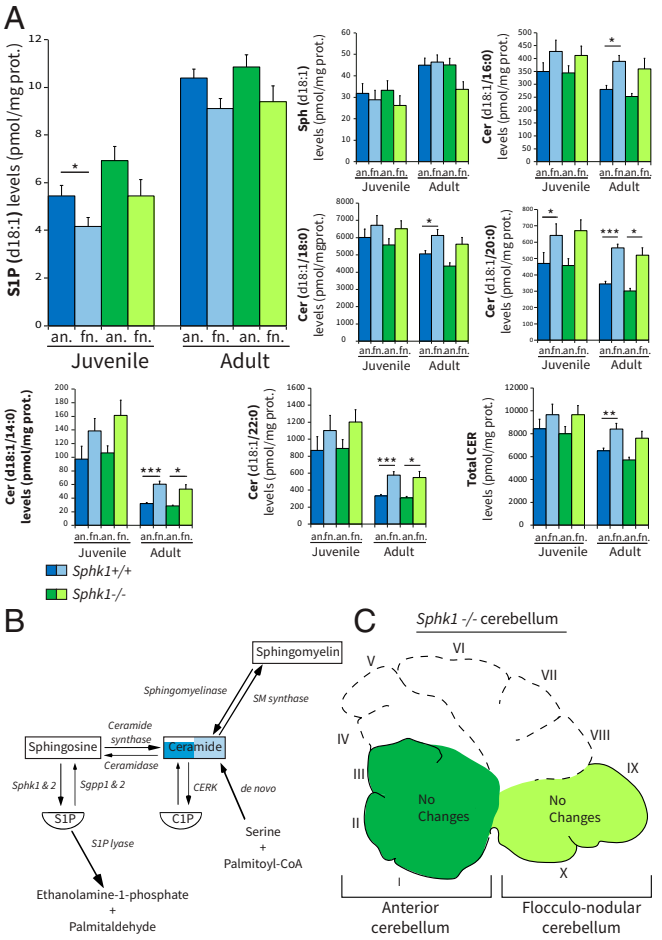

Fig. 3. Sphk1 deletion has marginal effects on sphingolipid levels in the cerebellum. (*A*) Bar plot of HPLC-MS/MS quantification of selected sphingolipid levels in wild-type *Sphk1*$^{+/+}$ (C57BL/6J) and mutant *Sphk1*$^{-/-}$ mice. (*B*) Schematic of the sphingolipid metabolic pathway with representation of level differences between anterior (dark blue) and flocculonodular (light blue) fractions. Difference between fractions for ceramides was based on total ceramide. (*C*) Schematic of the sagittal view of the *Sphk1*$^{-/-}$ cerebellum, with identification of the fractions and annotation of the sphingolipid changes measured in the adult mutant in independent fractions. Data are expressed as mean ± SEM ($n = 10$ per group); the unit is picomoles per milligram of protein. Juvenile indicates P21 to P23, and adult indicates P143 to P153. Statistical analyses for LC-MS/MS lipid quantification were performed using Levene's test for equality followed by Student's *t* test paired to compare anterior vs. flocculonodular fractions (black asterisks) and unpaired to compare *Sphk1*$^{+/+}$ vs. *Sphk1*$^{-/-}$, with Bonferroni correction for multiple comparisons. an., anterior; fn., flocculonodular; Cer/CER, ceramide; CERK, ceramide kinase; SM, sphingomyelin. *$P < 0.05$; **$P < 0.005$; ***$P < 0.001$.

S1P and Sph Levels Show a Significant Multiinteraction Effect of Age, Cerebellar Fraction, and Genotype. The extended lipidomic dataset we obtained allowed for further investigation of possible multiinteraction effects for all genotypes, ages, and cerebellar fractions. To this end, we performed a linear mixed model analysis and considered all interaction effects involving the fraction as a fixed effect (fraction × age; fraction × genotype; fraction × age × genotype). The significant statements previ-

ously established from Student's t tests with Bonferroni correction (Figs. 2 and 3) were verified and confirmed by the linear mixed model (95% CI in *SI Appendix*, Fig. S4). Of the 16 tested sphingolipids, only S1P(d18:1) ($P < 0.001$) and Sphk1(d18:1) ($P < 0.05$) had a significant multiinteraction effect for age × fraction × genotype. Together with the representation of the mean sphingolipid levels and the 95% CI (*SI Appendix*, Fig. S4), it showed that the considerable increase of S1P(d18:1) observed in the anterior fraction of adult *Atxn1[82Q]*/+ mice was the result of multiinteraction effect of age × fraction × genotype. For all other ceramides or sphingomyelins, no interaction effect of age × fraction × genotype was observed (all $P > 0.05$). We observed that only SM(d18:1/18:0) exhibited an interaction effect for fraction × age ($P < 0.05$), while the other sphingolipid levels did not show significance for either fraction × age or fraction × genotype interactions (all $P > 0.05$). These data confirmed that the changes for S1P(d18:1) observed in the *Atxn1[82Q]*/+ mice compared with wild-type mice cannot be attributed to random effects.

Sphk1 Deletion in the *Atxn1[82Q]/+* Mice Rescues Populations of PCs. Based on our sphingolipid analysis and the central role of S1P, we hypothesized that the increase of S1P contributes to the pathogenicity in the *Atxn1[82Q]*/+ mice. To investigate a potential benefit of reducing the Sphk activity, we deleted the *Sphk1* gene in *Atxn1[82Q]*/+ mice and analyzed the consequences on PC atrophy. We compared the pathology observed in the double mutant (*Atxn1[82Q]*/+; $Sphk1^{-/-}$) with the PC degeneration observed in the single mutant (*Atxn1[82Q]*/+; $Sphk1^{+/+}$) using CaBP expression and PC diameter as indicators of abnormal physiology, morphology, and PC degeneration (55). In single-mutant *Atxn1[82Q]*/+; $Sphk1^{+/+}$ mice, we observed a decrease of CaBP expression throughout the cerebellum compared with wild-type littermates *Atxn1[82Q]*/–; $Sphk1^{+/+}$ mice (Fig. 4*A*). The *Atxn1[82Q]*/+ transgene in the mixed FVB/N;C57BL/6-J background resulted in a phenotype similar to the original FVB/N background line (*SI Appendix*, Fig. S6). The fluorescence intensity profiles in lobule III and the cerebellar nuclei showed a clear reduction of CaBP expression compared with the expression in wild-type mice (*SI Appendix*, Fig. S5). In the double-mutant *Atxn1[82Q]*/+; $Sphk1^{-/-}$ mice, CaBP expression is partially preserved, indicating a rescue of PCs (Fig. 4*A* and *SI Appendix*, Figs. S5 and S6). However, this rescue was unequal throughout the cerebellum. The deletion of Sphk1 appears to protect the anterior cerebellum from neurodegeneration, while the posterior cerebellum remains seemingly as affected as in the single-mutant *Atxn1[82Q]*/–; $Sphk1^{+/+}$ mice (Fig. 4 and *SI Appendix*, Fig. S5*B*). This was consistently observed in each biological replicate ($n = 3$ per genotype) (*SI Appendix*, Fig. S6). As PC atrophy is a feature observed in early stages of the *Atxn1[82Q]*/+ neurodegenerative phenotype, we then measured PC diameter in their axial profile (Fig. 4*B*). The histogram distribution of PC sizes confirmed that in single-mutant mice, a high number of PCs showed atrophy (Fig. 4*C*) (relative to wild-type anterior hemispheres/anterior vermis/posterior: $P < 0.001$). The flocculonodular lobule was not affected in any genotype. In double-mutant *Atxn1[82Q]*/+; $Sphk1^{-/-}$ mice, the distribution of PC sizes significantly shifted away from the single mutant in the anterior cerebellum (anterior hemispheres: $P < 0.005$; anterior vermis: $P < 0.05$). In the anterior hemispheres, we found a distribution identical to that observed in wild-type mice, while in the anterior vermis, we found a bimodal distribution indicating that a subset of the PCs maintained a healthy morphology. In the posterior cerebellum, double-mutant *Atxn1[82Q]*/+; $Sphk1^{-/-}$ mice were not significantly different from the single-mutant *Atxn1[82Q]*/+; $Sphk1^{+/+}$, confirming a limited effect of the rescue in this region. For a clear visualization of the rescue effect, we established a threshold of PC diameter for each region based on the average cell size in wild-type mice minus one SD. In the anterior hemisphere, 71.1% (263/370 PCs) of the cells in double-mutant *Atxn1[82Q]*/+; $Sphk1^{-/-}$ mice were above this threshold, against 21.6% (69/366 PCs) in single-mutant *Atxn1[82Q]*/+; $Sphk1^{+/+}$ mice ($P < 0.0001$). Despite the increase, this value is still lower than the 86.7% (319/368 PCs) above the threshold of wild-type mice ($P < 0.005$). In the anterior vermis, PCs in double-mutant *Atxn1[82Q]*/+; $Sphk1^{-/-}$ mice significantly improve with 36.3% (193/532 PCs) above threshold against 13.5% (69/512 PCs) in single-mutant *Atxn1[82Q]*/+; $Sphk1^{-/-}$ mice ($P < 0.001$) (Fig. 4*D*, white asterisks). In the posterior region, we see a trend with 42.8% (161/376 PCs) of PCs above the threshold in double-mutant *Atxn1[82Q]*/+; $Sphk1^{-/-}$ mice against 34.4% (115/334 PCs) in single-mutant *Atxn1[82Q]*/+; $Sphk1^{-/-}$ mice ($P = 0.28$). We found no significant changes in the flocculonodular lobule between wild-type (84.9%; 464/546 PCs), single-mutant *Atxn1[82Q]*/+; $Sphk1^{+/+}$ (78.8%; 453/575 PCs), and double-mutant *Atxn1[82Q]*/+; $Sphk1^{-/-}$ (80.2%; 477/595 PCs) mice. From these results, we conclude that the deletion of Sphk1 results in the rescue of subpopulations of PCs from the pathological effect of the *Atxn1[82Q]* transgene expression.

Astrocyte and Microglia Activation Correlates with the Spatial Pattern of PC Degeneration. Previous studies showed that PC degeneration in *Atxn1[82Q]*/+ mice correlates with an early immune response progressing with the course of the pathology (56, 57). We investigated astrocyte and microglia activation in our rescue model via immunostaining for the glial fibrillary acidic protein (GFAP) and the allograft inflammatory factor 1 (Iba1) immunostaining, respectively, to test for potential changes in the immune response. In single-mutant *Atxn1[82Q]*/+; $Sphk1^{+/+}$ mice, we observed an overall increase of GFAP immunoreactivity, while in the double-mutant *Atxn1[82Q]*/+; $Sphk1^{-/-}$ mice, the intensity of GFAP immunoreactivity was variable (Fig. 5*A*). Domains of high CaBP expression exhibit low GFAP immunoreactivity, while domains with low CaBP immunoreactivity (i.e., altered PCs) showed a strong astrocytic response. Iba1 immunostaining revealed changes in the number of activated microglia in both anterior and posterior regions (one-way ANOVA, both $P < 0.001$). No significant change in the number of activated microglia was observed in the flocculonodular among the three genotypes, which showed that at this age the flocculonodular lobule is relatively spared from the immune response in the *Atxn1[82Q]*/+ model (one-way ANOVA, $P = 0.17$). In single-mutant *Atxn1[82Q]*/+; $Sphk1^{+/+}$ mice, the post hoc analysis showed a significant increase in activated microglia in both anterior and posterior regions (Fig. 5 *B* and *C*) (both $P < 0.001$). In double-mutant *Atxn1[82Q]*/+; $Sphk1^{-/-}$ mice, we observed a relative decrease in the number of activated microglia compared with the single mutant. This decrease in *Atxn1[82Q]*/+; $Sphk1^{-/-}$ mice compared with *Atxn1[82Q]*/+; $Sphk1^{+/+}$ mice was more pronounced in the anterior (7.8 ± 0.3 vs. 14.3 ± 0.6 Iba1+ cells in 0.04 mm^2; $P < 0.001$) than the posterior cerebellum (10.4 ± 0.6 vs. 13.5 ± 0.8 Iba1+ cells in 0.04 mm^2; $P < 0.05$). Nevertheless, the number of Iba+ microglia remained significantly higher than the wild-type littermates in both regions (both $P < 0.001$). These data show that the glial activation correlates precisely with the severity and the spatial pattern of the degeneration.

Deletion of Sphk1 in *Atxn1[82Q]/+* Mice Rescues Parasagittal Domains of PCs. In double-mutant *Atxn1[82Q]*/+; $Sphk1^{-/-}$ mice, rescued PCs appear to be clustered in bands in the

NEUROSCIENCE

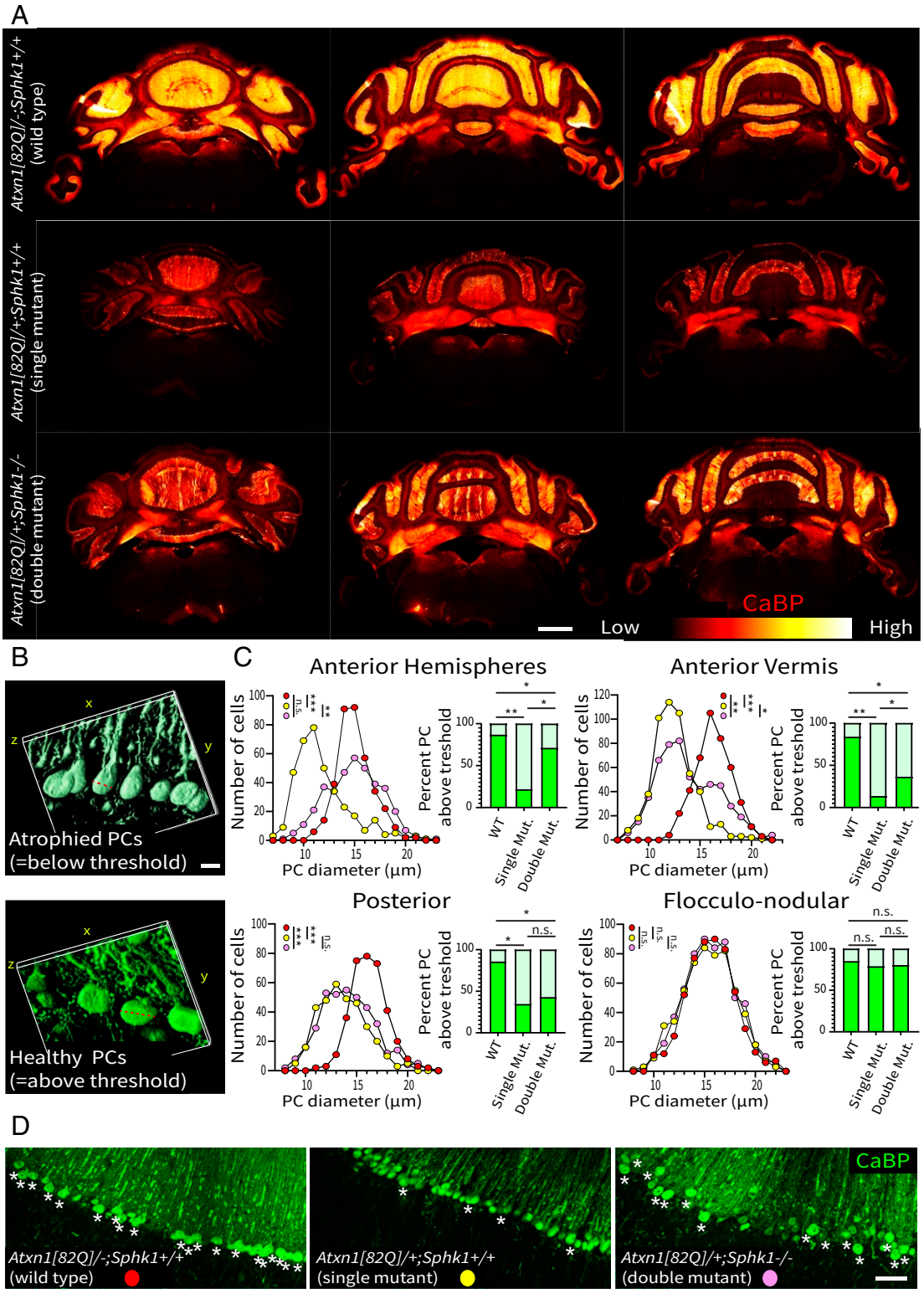

Fig. 4. Deletion of Sphk1 in *Atxn1[82Q]/+* mice partially rescues PC degeneration. (*A*) Overviews of the example cerebella immunostained for CaBP in wild-type (*Atxn1[82Q]/—*; *Sphk1*$^{+/+}$), single-mutant (*Atxn1[82Q]/+; Sphk1*$^{+/+}$), and double-mutant (*Atxn1[82Q]/+; Sphk1*$^{-/-}$) mice. CaBP expression levels are represented by the heat map, from low (red) to high expression levels (white). (Scale bar: 1 mm.) (*B*) The three-dimensional reconstruction and measurement of soma size (red dotted lines) of atrophied PCs imaged in single-mutant mice (*Upper*; PC diameter = 11.7 μm) and healthy PCs in double-mutant mice (*Lower*; PC diameter = 17.3 μm) in the vermis. (Scale bar: 10 μm.) (*C*) Histograms of PC soma size in wild-type (red), single-mutant *Atxn1[82Q]/+*; *Sphk1*$^{+/+}$ (yellow), and double-mutant *Atxn1[82Q]/+*; *Sphk1*$^{-/-}$ (pink) mice. Bar graphs show the percentage of PCs above/below the threshold (dark/light green, respectively) defined by the average of wild-type PC size minus one SD for each region (anterior hemisphere = 13.3 μm, anterior vermis = 14.6 μm, posterior = 14.4 μm, flocculonodular = 13.2 μm). PC diameters were compared using a one-way ANOVA corrected for multiple comparisons (Dunn's correction). The percentage of PC diameters above the wild-type threshold was compared with a Kruskal–Wallis rank sum test for multiple independent samples. *$P < 0.05$; **$P < 0.005$; ***$P < 0.001$. (*D*) High magnification of PCs in the anterior vermis illustrating the percentage of cells with a diameter above the threshold (white asterisks). WT, wild-type; Mut., mutant; n.s, not significant. (Scale bar: 50 μm.)

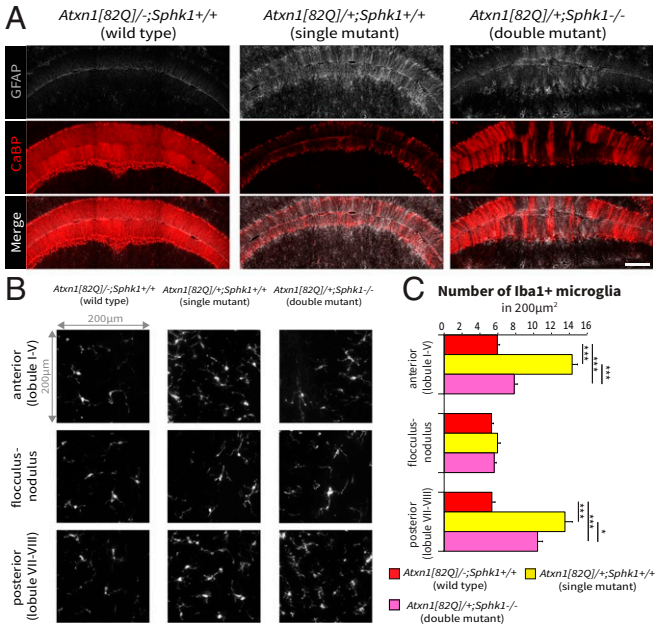

Fig. 5. Immune response correlates with the severity of PCs degeneration. (*A*) Immunostaining for GFAP (gray) and CaBP (red) proteins in the wild-type (*Atxn1[82Q]/–; Sphk1*$^{+/+}$), single-mutant (*Atxn1[82Q]/+; Sphk1*$^{+/+}$), and double-mutant (*Atxn1[82Q]/+; Sphk1*$^{-/-}$) mice. (Scale bar: 200 μm.) (*B*) Iba1+ microglia density in a window of 200 × 200 μm in three regions: the anterior (lobules I to V), the posterior (lobules VI and VII), and the flocculonodular cerebellum. (*C*) Quantification of Iba1+ microglia in a window of 200 × 200 μm. Number of samples: three regions of interest per section, three sections per region, and three mice per genotype. Statistical analyses for activated microglia counting were performed with one-way ANOVA and post hoc analysis with Bonferroni correction to compare all genotypes (black asterisks). *$P < 0.05$; ***$P < 0.001$.

transverse plane along the cortex (Fig. 4*A* and *SI Appendix*, Fig. S6*A*), reminiscent of the cerebellar modules. We used immunostaining for AldoC to identify the rescued subpopulations of PC distributed in parasagittal domains. Comparing the profile of CaBP expression with the AldoC pattern showed that rescued PC domains in the *Atxn1[82Q]/+; Sphk1*$^{-/-}$ double mutant partially match with the AldoC-positive bands observed in the wild-type *Atxn1[82Q]/–; Sphk1*$^{+/+}$ mice (Fig. 6 *A* and *C* and *SI Appendix*, Fig. S7). For example, in the vermis of the double mutant, we observed that rescued regions, identified by CaBP expression, correspond to the parasagittal domains 1+/2+/3+ as defined by the AldoC immunostaining in the wild type (Fig. 6*A* and *SI Appendix*, Fig. S7). However, PC rescue was not limited to the AldoC-positive domains, as the domain 3– also exhibited high levels of CaBP expression. The pattern of rescue was consistent in all biological replicates (*SI Appendix*, Fig. S6). In single-mutant *Atxn1[82Q]/+; Sphk1*$^{+/+}$ mice, we observed that the AldoC expression was mostly disrupted (Fig. 6 *A* and *B*) across the cerebellum, and only lobule X, CrusI, and Flocculus retained an expression relatively identical to the wild-type animals (46). In contrast, double-mutant *Atxn1[82Q]/+; Sphk1*$^{-/-}$ mice partially recovered AldoC expression, primarily in the anterior cerebellum (Fig. 5 *A*, *Bottom* and *B*, *Bottom*). In the posterior cerebellum (lobules VII/VIII/IX) despite signs of AldoC expression recovery, the pattern remained heavily disrupted (Fig. 5 *B*, *Top*). Interestingly, while we observed that CaBP expression recovery, a sign of rescue, appeared predominantly in putative AldoC-positive domains, AldoC expression is not systematically recovered (Fig. 6*C*). This indicates that AldoC expression is not a sine qua non condition of PC rescue. These results demonstrate that Sphk1 deletion in the *Atxn1[82Q]*/+ leads to survival of PCs preferentially but not exclusively in AldoC-positive domains and that AldoC expression is partly recovered but is not an absolute requirement for PC survival (Fig. 6*D*).

Sphk1 Deletion Affects ATXN1[82Q] Protein Expression in Subpopulations of PCs. The PC degeneration observed in the *Atxn1[82Q]*/+ model is caused by the expression and nuclear localization of the mutant ATXN1[82Q] protein (47). We compared ATXN1 expression in both single *Atxn1[82Q]*/+; *Sphk1*$^{+/+}$ and double *Atxn1[82Q]*/+; *Sphk1*$^{-/-}$ mutant mice using anti-ATXN1 antibody (antibody 11750) to examine the expression and subcellular localization of the mutant protein between the disease model and the rescue, using the 11750 antibody that labels both the endogenous and mutant proteins (58). In single-mutant *Atxn1[82Q]/+; Sphk1*$^{+/+}$ mice, we observed two clearly distinct types of PCs:

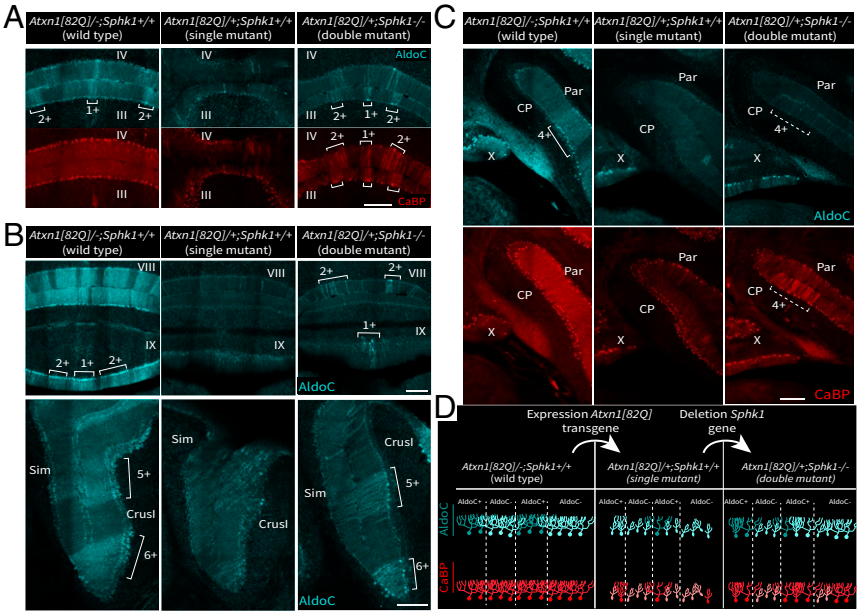

Fig. 6. Rescued PC population in the double-mutant correlates with cerebellar modules defined by the AldoC pattern. (*A–C*) Coimmunostaining for AldoC protein and CaBP in wild-type (*Atxn1[82Q]/–; Sphk1*$^{+/+}$), single-mutant (*Atxn1[82Q]/+; Sphk1*$^{+/+}$), and double-mutant (*Atxn1[82Q]/+; Sphk1*$^{-/-}$) mice; 1+/2+/3+/4+/5+/6+ indicate domains of high AldoC expression as defined by Sugihara and Quy (9). Dashed lines indicate putative AldoC-positive domain. (*D*) Schematic representation of CaBP (red) and AldoC (cyan) expression in the PC layer comparing wild-type cerebella with pathological cerebella following expression of Atxn1[82Q] transgene expression and rescued PCs following Atxn1[82Q] transgene expression together with Sphk1 deletion. Cyan indicates AldoC, and red indicates CaBP. CP, copula pyramidis; Par, paramedian lobule; Sim, simplex lobule. (Scale bars: 200 μm.)

low-ATXN1/high-CaBP PCs (Fig. 7*A*, white asterisks) or high–nuclear ATXN1/low-CaBP PCs (Fig. 7*A*, blue arrowheads). The first type resembled the expression levels of ATXN1 observed in wild-type mice. The second type exhibits anti-ATXN1 reactivity in PC nuclei that is due to the expression of the mutant ATXN1[82Q] protein (47). In double-mutant *Atxn1[82Q]/+; Sphk1*$^{-/-}$ mice, we observed the same two types of PCs, but the proportion of high–nuclear ATXN1/low-CaBP PCs was diminished (Fig. 7*A*, blue arrowheads). In both genotypes, we investigated the relationship between high–nuclear ATXN1 immunoreactivity and PC atrophy (Fig. 7*A*). In single-mutant *Atxn1[82Q]/+*; *Sphk1*$^{+/+}$ mice, high–nuclear ATXN1/low-CaBP PCs presented a significantly smaller diameter (12.2 ± 0.2 μm for 70 PCs) then low-ATXN1/high-CaBP PCs (17.6 ± 0.3 μm for 46 PCs; $P < 0.0001$). Similar values were observed in the double-mutant *Atxn1[82Q]/+*; *Sphk1*$^{-/-}$ mice (12.6 ± 0.1 μm for 65 PCs and 19.4 ± 0.2 μm for 50 PCs, respectively; $P < 0.0001$). These data clearly demonstrate that high nuclear immunoreactivity for ATXN1 correlated with PC atrophy in both genotypes. Interestingly, low-ATXN1/high-CaBP PC populations were significantly different between both genotypes ($P < 0.0001$), as the data reveal a broader range of sizes, or the existence of two populations of different sizes, in the single-mutant *Atxn1[82Q]/+*; *Sphk1*$^{+/+}$ mice (Fig. 7*B*). This suggest that signs of atrophy might appear prior to detectable levels of ATXN1[82Q] protein in the nucleus. We conclude that the deletion of Sphk1 in *Atxn1[82Q]/+* abolished the expression of the ATXN1[82Q] protein in a subset of PCs, putatively preventing the degeneration of specific subsets of PCs.

Discussion

In the present study, we provide a comprehensive analysis of region-specific differences in sphingolipid metabolism in the cerebellar cortex, its alterations in a mouse model for SCA1, and its implication in PC fate and patterned degeneration. In healthy cerebella, we found differential levels of Sphk1 as well as S1P between the anterior and flocculonodular regions. We showed that while expression of both enzymes decreases in the *Atxn1[82Q]/+* mice, S1P levels increase significantly and predominantly in the anterior region, where neurodegeneration is prevalent. Finally, we showed that Sphk1 deletion selectively rescues cerebellar domains in the *Atxn1[82Q]/+* mice as it abolishes ATXN1[82Q] protein nuclear accumulation in a subset of PCs. Our data support the concept of an essential role of the sphingolipid metabolism in neuronal survival in the *Atxn1[82Q]/+* model. In healthy cerebella, Sphk1 expression levels were higher in the flocculonodular than in the anterior region, confirming a previous report (51), while Sphk2 expression levels were comparable between cerebellar regions. Although S1P is the product of the enzymatic reaction catalyzed by Sphk1 and Sphk1 levels were lower in the anterior region, the S1P levels were higher in the anterior region of adult animals compared with the flocculonodular region. A similar trend was observed in C57BL/6-J control lines, indicating that this is a consistent feature of cerebellar lipid homeostasis in mice. We also observed that *Sphk1* gene deletion had no significant impact on regional S1P levels. This suggests that regional S1P levels are not only the result of Sphk1 differential expression but also depend on other enzymes in this pathway expressed differentially in the cerebellar cortex. A recently published high–spatial resolution single-cell RNA sequencing study (59) listed 669 genes with nonhomogeneous expression in the PC layer, highlighting different patterns of expression in the cerebellar cortex. Among the reported genes were ceramide kinase, ceramide synthase 4, sphingomyelin phosphodiesterase 1, and Sphk1 interactor. Taken together, this highlights the existence of regional molecular mechanisms to maintain the adequate level of sphingolipids, resulting in a local tight control of S1P metabolism in healthy physiological condition. As an essential driver of cellular fate, S1P physiological levels play a role in the selective vulnerabilities to neuropathological insults commonly observed. Previous studies showed correlations between sphingolipid dyshomeostasis and cerebellar ataxia pathologies in mouse (38–40, 44, 60, 61) and human (53). In this work, we investigate sphingolipid metabolism in a mouse model for SCA1. In *Atxn1[82Q]/+* mice, we found that sphingolipid levels correlate with the progression of the neurodegeneration. In this model, no discernible signs of neurodegeneration can be observed in juvenile animals (46), while adult mice exhibit severe neurodegeneration, predominantly in the anterior cerebellum. In juvenile *Atxn1[82Q]/+* mice, sphingolipids and the two kinases, Sphk1 and Sphk2, were not significantly changed, in line with the absence of a neurodegenerative phenotype. In adult mutant mice, Sphk1 expression levels decreased in the flocculonodular region, while Sphk2 expression levels decreased in both anterior and flocculonodular regions, with a predominant decrease in the anterior cerebellum. In parallel, we observed that S1P levels increased in both regions with a predominant change in the anterior cerebellum. In addition to S1P, C16 ceramide and SM16/18/18:1 sphingomyelin levels change in the *Atxn1[82Q]/+* mice, all specifically in the anterior region, which is primarily compromised by neurodegeneration. Surprisingly, specific increase of C16 ceramide was also observed through the course of Alzheimer's disease pathogenesis and was previously associated with Sphk2 loss of activity (62, 63). The balance between ceramide and S1P controls cellular apoptosis, as defined by the "sphingolipid rheostat" concept (33, 64). However, in the cerebellum, accumulation of long-chain bases correlates with neurodegeneration (35, 45), as S1P can act as a proapoptotic mediator independently from the ceramide levels (42). The cellular fate driven by S1P is thought to be dependent on the kinase in play and therefore, its subcellular localization (42). Hence, the overall increase of S1P that we found in the cerebellum

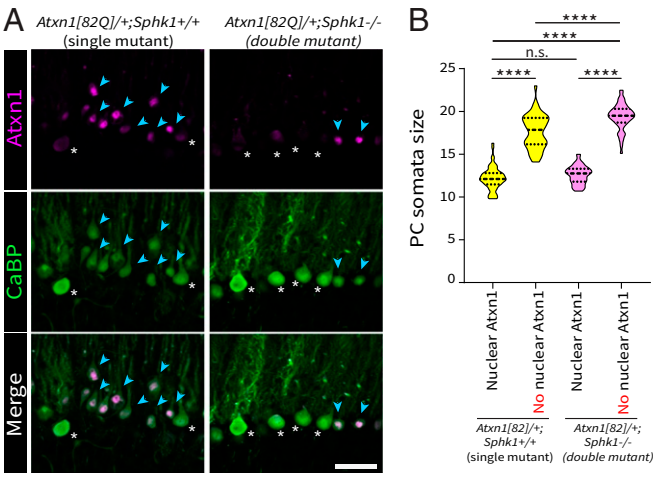

Fig. 7. Sphk1 deletion abolishes ATXN1[82Q] protein expression in subsets of PCs. (*A*) Detection of endogenous ATXN1 and mutant ATXN1[82Q] protein with anti-ATXN1 antibody 11750 (purple) and with immunostaining for CaBP protein (green) in single-mutant (*Atxn1[82Q]/+; Sphk1*$^{+/+}$) and double-mutant (*Atxn1[82Q]/+; Sphk1*$^{-/-}$) mice. Two main types of PCs are shown: low ATXN1/high CaBP (white asterisks) and high nuclear ATXN1/low CaBP (blue arrowheads). (Scale bar: 50 μm.) (*B*) Violin plot of PCs somata diameter with nuclear or with no nuclear high immunoreactivity of ATXN1 in both single-mutant (*Atxn1[82Q]/+; Sphk1*$^{+/+}$) and double-mutant (*Atxn1[82Q]/+; Sphk1*$^{-/-}$) mice. PC diameters were compared using a one-way ANOVA corrected for multiple comparisons (Dunn's correction). ****$P < 0.001$. n.s., not significant.

of *Atxn1[82Q]*/+ mice could be interpreted either as a cause or as a response to the neurodegeneration. Is S1P an efficient proapoptotic mediator or an ineffective neuroprotective agent? As the region primarily affected by the pathology, the anterior cerebellum, exhibits higher S1P levels compared with the region preserved from the neuropathology (flocculonodular cerebellum), our working hypothesis was that in *Atxn1[82Q]*/+ mice, the increase of S1P has a proapoptotic effect. Indeed, we found that deletion of Sphk1 in *Atxn1[82Q]*/+ mutant mice improves the survival of PC, as observed with CaBP expression, PCs atrophy, and microglia activation, used as a readout for the spatiotemporal pattern of cerebellar neurodegeneration (50, 56). In Allende et al. (54), the authors found that in $Sphk1^{-/-}$ mice, the kinase activity and S1P synthesis in brain homogenate were maintained at normal physiological levels and suggested that this was due to compensatory activity of Sphk2, a redundancy that explains why we did not observe a change in S1P levels in the $Sphk1^{-/-}$ mice. In our double-mutant *Atxn1[82Q]*/+; $Sphk1^{-/-}$ mice, this compensatory mechanism is unlikely, as we observed an overall decrease of Sphk2 in the *Atxn1[82Q]*/+ mice. The loss of Sphk1 and the down-regulation of Sphk2 would arguably impair S1P synthesis. Our data do not allow us to conclude whether PC rescue resulted from a different subcellular localization of S1P due to the sole activity of Sphk2 or an overall decrease of S1P levels. Yet, we confirm that Sphks, and therefore, S1P metabolism, contribute to PC degeneration in *Atxn1[82Q]*/+ mice. The measures of CaBP expression levels, PCs diameter, and activated microglia in the cerebellar cortex all showed a complex pattern of rescue in double-mutant *Atxn1[82Q]*/+; $Sphk1^{-/-}$ mice. Sphk1 deletion rescued PCs in the anterior cerebellum, predominantly, but not exclusively, in parasagittal bands reminiscent of the known AldoC-positive domains. The idea that AldoC expression is a determinant factor for PC survival has been addressed for many pathologies (24). However, here the survival is not restricted to AldoC-positive PCs domains as we also observed some AldoC-negative PCs being rescued in the double mutant. We also reported that PCs rescued in putative AldoC-positive domain do not systematically recover a proper AldoC expression. These data suggest that AldoC differential expression is not the direct cause of preferential survival. It was previously established that Sphk1 protein is expressed in a pattern similar to AldoC expression in the cerebellum (51), which partially explains the parasagittal pattern of rescued PCs observed in double-mutant mice. The consequences of Sphk1 deletion still need to be elucidated to fully understand the PC subtype selectivity and the mechanism(s) behind the rescue. In the present study, we show that Sphk1 deletion impacts ATXN1[82Q] mutant protein expression. Previous work established that the SCA1 model is a proteinopathy caused by the localization of ATXN1[82Q] mutant protein in the nucleus (47). The role of sphingolipid metabolism in proteinopathies is an emerging concept in the field of neurodegenerative disorders. Evidence for sphingolipid dyshomeostasis has been observed in the brain tissue of Parkinson's, Alzheimer's, and Huntington's disease patients and/or mouse models, where sphingolipids are impacted both in their structural role at the membranes and in their bioactive role in signal transduction, which consequently acted on misfolded proteins (65). The cellular cascade downstream of S1P receptors is known to directly impact several transcriptional processes, which could explain changes in ATXN1[82Q] expression. It has also been showed that the stability of ATXN1 protein depends on the phosphorylation activity of Akt1 (66), a phosphatase known as an essential transducer of S1P receptor–mediated signal. Additional experiments are necessary to fully explain the observed cellular phenotype. Here, we show that Sphk1 deletion has beneficial effects on neuronal survival. Our work reveals upstream pathways of neurotoxicity in the *Atxn1[82Q]*/+, which could be valuable to understand selective neurodegeneration in general. However, we do not exclude other potential mechanisms also involved in the regional sensitivity observed in multiple cerebellar diseases (24, 25) We conclude that 1) sphingolipid metabolism is controlled locally, depending on the molecular identity of PCs; 2) Sphks and related lipid levels are affected in a mouse model for cerebellar neurodegeneration; and 3) deletion of a main Sphk, Sphk1, is able to partially rescue the degeneration as it abolishes the expression of the ATXN1[82Q] protein. These data support a central role of sphingolipid metabolism in neurodegeneration and support the therapeutic perspectives that sphingolipid pathway modulators could offer (67–69).

Materials and Methods

Animals. *Atxn1[82Q]*/+ mice originated from the transgenic line B05, originally created by Burright et al. (52), and were kindly provided by Harry T. Orr, Department of Laboratory Medicine and Pathology, Institute for Translational Neuroscience, University of Minnesota, Minneapolis, MN. The line was maintained in an FVB/N background. $Sphk1^{-/-}$ mice (54) were purchased from The Jackson Laboratory and were maintained in a C57BL/6-J background. *Atxn1[82Q]*/+ and $Sphk1^{-/-}$ lines were crossed to obtain *Atxn1[82Q]*/—; $Sphk1^{-/+}$ and *Atxn1[82Q]*/+; $Sphk1^{-/+}$ mice (= F1). *Atxn1[82Q]*/+; $Sphk1^{-/+}$ mice were then inbred to obtain *Atxn1[82Q]*/—; $Sphk1^{+/+}$ (wild-type), *Atxn1[82Q]*/+; $Sphk1^{+/+}$ (single-mutant), and *Atxn1[82Q]*/+; $Sphk1^{-/-}$ (double-mutant) mice (= F2). Mice were randomly housed together with two to four siblings of the same sex, both mutants and controls. Male and female *Atxn1[82Q]*/+ and $Sphk1^{-/-}$ and their wild-type littermates were tested between age P21 and P23 (juvenile) or between P143 and P153 (adult). All experiment protocols were approved by the institutional welfare committee of the Erasmus Medical Center.

HPLC-MS/MS. We quantified selected sphingolipid levels using HPLC-MS/MS. Cerebella were obtained from juveniles (n = 10 per group) and adults (n = 10 per group) and extracted as previously described. In each sample, sphingolipids were extracted as previously described by Hoogendoorn et al. (70). Frozen cerebellar samples were homogenized in cold Millipore water (MQ, 18.2 M cm) from a Milli-Q PF plus system (Millipore B.V.) up to 10 μL samples. The internal standards Cer(d18:1/17:0), Cer(d17:0/24:1), and S1P(d18:1)-D7 were added (10 μL 2, 2, and 0.2 μg/mL in methanol, respectively; internal standards: Avanti Polar Lipids; methanol: Merck Millipore B.V.). After addition of 10 μL 10% triethanolamine solution [TEA; [10:90, vol/vol] in methanol/dichloromethane [DCM; 50:50, vol/vol]; TEA: Merck Millipore B.V.; DCM: Merck Millipore B.V.), lipids were extracted with 450 μL methanol/DCM (50:50, vol/vol). Samples were vortexed and incubated under constant agitation for 30 min at 4 °C followed by centrifugation at 18,500 × g for 20 min at 4 °C (Hettich mikro 200R). Supernatants were transferred to glass vials, freeze dried, and reconstituted in 100 μL methanol before liquid chromatography–tandem mass spectrometry (LC-MS/MS). LC-MS/MS analysis was performed as previously described (70) on a Sciex Qtrap 5500 quadruple mass spectrometer (AB Sciex Inc.). S1P, Sph, and the seven most abundant ceramide species for which standards were commercially available were analyzed. Nine-point calibration curves were constructed by plotting analyte to internal standard peak area ratios for Cer(d18:1/14:0), Cer(d18:1/16:0), Cer(d18:1/18:0), Cer(d18:1/20:0), Cer(d18:1/22:0), Cer(d18:1/24:1), Cer(d18:1/24:0), Sph, and S1P(d18:1) (all Avanti polar lipids). Instrument control and quantification of spectral data were performed using MultiQuant software (AB Sciex Inc.). Cerebellum sphingolipid levels were normalized to protein content obtained by bicinchoninic acid assay.

Histology. Animals were deeply anesthetized through intraperitoneal administration of sodium pentobarbital (60 mg/mL), directly followed by transcardial perfusion with 4% paraformaldehyde (PFA) in 0.12 M phosphate buffer (PB), pH 7.6. Brains were postfixed for 1 h in 4% PFA at room temperature (rT) and transferred to 10% sucrose solution overnight at 4 °C. The cerebella were embedded in a 10% gelatin (FUJIFILM Wako Pure Chemicals):10% sucrose mix, and gelatin blocks were incubated in 30% sucrose:10% formaldehyde for 2 h at rT and incubated overnight in 30% sucrose at 4 °C. Subsequently, coronal sections were cut at a 40-μm thickness with freezing microtome. Free-floating sections were rinsed with 0.1 M PB and incubated in 10 mM sodium citrate (pH 6) at 80 °C for 2 h for antigen

retrieval. For immunofluorescence, sections were rinsed with 0.1 M PB, followed by three washes of 10 min in phosphate buffered saline (PBS). Then, sections were incubated for 90 min at rT in a solution of PBS:0.5%Triton-X100:10% normal horse serum (NHS) to block nonspecific protein-binding sites and incubated for 48 h at 4 °C in a solution of PBS:0.4% Triton-X100:2% NHS, with primary antibodies diluted as follows: CaBP 1:14,000 (rabbit polyclonal, CB-38a; Swant), AldoC 1:500 (goat polyclonal, SC-12065; Santa Cruz Biotechnology), GFAP 1:1,000 (chicken polyclonal, 4674; Abcam), Iba1 1:1,000 (rabbit polyclonal, 019–19741; WAKO), and ATXN1 1:4,000 [rabbit polyclonal, 11750 (47); kindly provided by Huda Zoghbi, Jan and Dan Duncan Neurological Research Institute, Texas Children's Hospital, Houston, TX; Departments of Molecular and Human Genetics and Pediatrics, Baylor College of Medicine, Houston, TX; and Howard Hughes Medical Institute, Houston, TX]. After rinsing in PBS, sections were incubated for 2 h at rT in PBS:0.4% Triton-X100:2% NHS solution with secondary antibodies coupled with Alexa488, Cy3, or Cy5 (1:1,000; Jackson ImmunoResearch). Sections were mounted on coverslips in a solution of gelatin/chrome alum and covered with Mowiol (Polysciences Inc.). For light microscopy, sections were pretreated for endogenous peroxidase activity blocking with 3% H_2O_2 in PBS, then rinsed for 30 min in PBS, and incubated for 90 min in a solution of PBS:0.5%Triton-X100:10% NHS, followed by the primary antibody incubation as described before. After 48 h, sections were rinsed in PBS and incubated for 2 h at rT in PBS:0.4% Triton-X100:10% NHS solution with HRP-coupled secondary antibodies (1:1,000; Jackson ImmunoResearch). Sections were rinsed with 0.1 M PB and incubated in diaminobenzidine (75 mg/100 mL) for 10 min. Sections were mounted on glass slides in a solution of gelatin/chrome alum, counterstained with Thionin dehydrated with successive ethanol steps (two times 96%, three times 100%), incubated in Xylene, and covered with Permount mounting medium (Fisher Chemical).

Data Availability. All study data are included in the article and/or supporting information. Details of the western blot method, image acquisition, behavioral tests, and statistical analysis are provided in *SI Appendix*, *SI Methods*.

ACKNOWLEDGMENTS. We thank Dr. Dick Jaarsma for his feedback and years of mentorship of F.G.C.B.; Dr. Harry T. Orr, who provided the Atxn1[82Q]/+ mice; Dr. Huda Zhogbi, who provided the anti-ATXN1 antibody; Dr. Chris I. De Zeeuw, Dr. Laurens W. J. Bosman, and Bram W. Kuppens for their cooperative work on the Atxn1[82Q]/+ mice; the board members of the Sphingolipid Club for providing an open environment for biochemists and nonbiochemists; and Laura Post for technical assistance. This work was supported by Nederlandse organisatie voor Wetenschappelijk Onderzoek NWO-ZonMw (to C.O.) and NWO-Veni (to J.J.W.) and European Research Council Starter Grant ERC-Stg 680235 (to M.S.).

1. N. L. Cerminara, E. J. Lang, R. V. Sillitoe, R. Apps, Redefining the cerebellar cortex as an assembly of non-uniform Purkinje cell microcircuits. *Nat. Rev. Neurosci.* **16**, 79–93 (2015).
2. D. M. Armstrong, R. F. Schild, A quantitative study of the Purkinje cells in the cerebellum of the albino rat. *J. Comp. Neurol.* **139**, 449–456 (1970).
3. H. Nedelescu, M. Abdelhack, Comparative morphology of dendritic arbors in populations of Purkinje cells in mouse sulcus and apex. *Neural Plast.* **2013**, 948587 (2013).
4. U. Müller, H. Heinsen, Regional differences in the ultrastructure of Purkinje cells of the rat. *Cell Tissue Res.* **235**, 91–98 (1984).
5. J. Voogd, Cerebellar zones: A personal history. *Cerebellum* **10**, 334–350 (2011).
6. G. Brochu, L. Maler, R. Hawkes, Zebrin II: A polypeptide antigen expressed selectively by Purkinje cells reveals compartments in rat and fish cerebellum. *J. Comp. Neurol.* **291**, 538–552 (1990).
7. Y. Dehnes *et al*., The glutamate transporter EAAT4 in rat cerebellar Purkinje cells: A glutamate-gated chloride channel concentrated near the synapse in parts of the dendritic membrane facing astroglia. *J. Neurosci.* **18**, 3606–3619 (1998).
8. J. R. Sarna, H. Marzban, M. Watanabe, R. Hawkes, Complementary stripes of phospholipase Cbeta3 and Cbeta4 expression by Purkinje cell subsets in the mouse cerebellum. *J. Comp. Neurol.* **496**, 303–313 (2006).
9. I. Sugihara, P. N. Quy, Identification of aldolase C compartments in the mouse cerebellar cortex by olivocerebellar labeling. *J. Comp. Neurol.* **500**, 1076–1092 (2007).
10. H. Zhou *et al*., Cerebellar modules operate at different frequencies. *eLife* **3**, e02536 (2014).
11. B. Wu *et al*., TRPC3 is a major contributor to functional heterogeneity of cerebellar Purkinje cells. *eLife* **8**, e45590 (2019).
12. J. I. Wadiche, C. E. Jahr, Patterned expression of Purkinje cell glutamate transporters controls synaptic plasticity. *Nat. Neurosci.* **8**, 1329–1334 (2005).
13. S. A. Gebre, S. L. Reeber, R. V. Sillitoe, Parasagittal compartmentation of cerebellar mossy fibers as revealed by the patterned expression of vesicular glutamate transporters VGLUT1 and VGLUT2. *Brain Struct. Funct.* **217**, 165–180 (2012).
14. J. Voogd, T. J. H. Ruigrok, The organization of the corticonuclear and olivocerebellar climbing fiber projections to the rat cerebellar vermis: The congruence of projection zones and the zebrin pattern. *J. Neurocytol.* **33**, 5–21 (2004).
15. J. A. Heckroth, L. C. Abbott, Purkinje cell loss from alternating sagittal zones in the cerebellum of leaner mutant mice. *Brain Res.* **658**, 93–104 (1994).
16. S. H. Chung, M. Calafiore, J. M. Plane, D. E. Pleasure, W. Deng, Apoptosis inducing factor deficiency causes reduced mitofusion 1 expression and patterned Purkinje cell degeneration. *Neurobiol. Dis.* **41**, 445–457 (2011).
17. J. R. Sarna, R. Hawkes, Patterned Purkinje cell loss in the ataxic sticky mouse. *Eur. J. Neurosci.* **34**, 79–86 (2011).
18. P. Strømme *et al*., X-linked Angelman-like syndrome caused by Slc9a6 knockout in mice exhibits evidence of endosomal-lysosomal dysfunction. *Brain* **134**, 3369–3383 (2011).
19. T. Miyazaki *et al*., $Ca_V2.1$ in cerebellar Purkinje cells regulates competitive excitatory synaptic wiring, cell survival, and cerebellar biochemical compartmentalization. *J. Neurosci.* **32**, 1311–1328 (2012).
20. J. P. Welsh *et al*., Why do Purkinje cells die so easily after global brain ischemia? Aldolase C, EAAT4, and the cerebellar contribution to posthypoxic myoclonus. *Adv. Neurol.* **89**, 331–359 (2002).
21. B. L. Williams, K. Yaddanapudi, M. Hornig, W. I. Lipkin, Spatiotemporal analysis of Purkinje cell degeneration relative to parasagittal expression domains in a model of neonatal viral infection. *J. Virol.* **81**, 2675–2687 (2007).
22. A. Ragagnin *et al*., Cerebellar compartmentation of prion pathogenesis. *Brain Pathol.* **28**, 240–263 (2018).
23. J. H. Lee, S. H. Heo, D. I. Chang, Early-stage alcoholic cerebellar degeneration: Diagnostic imaging clues. *J. Korean Med. Sci.* **30**, 1539 (2015).
24. J. R. Sarna, R. Hawkes, Patterned Purkinje cell death in the cerebellum. *Prog. Neurobiol.* **70**, 473–507 (2003).
25. C. Chung *et al*., Heat shock protein beta-1 modifies anterior to posterior Purkinje cell vulnerability in a mouse model of Niemann-Pick type C disease. *PLoS Genet.* **12**, e1006042 (2016).
26. I. Ishii, N. Fukushima, X. Ye, J. Chun, Lysophospholipid receptors: Signaling and biology. *Annu. Rev. Biochem.* **73**, 321–354 (2004).
27. A. Olivera *et al*., Sphingosine kinase expression increases intracellular sphingosine-1-phosphate and promotes cell growth and survival. *J. Cell Biol.* **147**, 545–558 (1999).
28. K. Mizugishi *et al*., Essential role for sphingosine kinases in neural and vascular development. *Mol. Cell. Biol.* **25**, 11113–11121 (2005).
29. T. Kanno *et al*., Regulation of synaptic strength by sphingosine 1-phosphate in the hippocampus. *Neuroscience* **171**, 973–980 (2010).
30. J. Chun *et al*., International Union of Pharmacology. XXXIV. Lysophospholipid receptor nomenclature. *Pharmacol. Rev.* **54**, 265–269 (2002).
31. A. Kihara, S. Mitsutake, Y. Mizutani, Y. Igarashi, Metabolism and biological functions of two phosphorylated sphingolipids, sphingosine 1-phosphate and ceramide 1-phosphate. *Prog. Lipid Res.* **46**, 126–144 (2007).
32. T. A. Taha, T. D. Mullen, L. M. Obeid, A house divided: Ceramide, sphingosine, and sphingosine-1-phosphate in programmed cell death. *Biochim. Biophys. Acta* **1758**, 2027–2036 (2006).
33. J. Newton, S. Lima, M. Maceyka, S. Spiegel, Revisiting the sphingolipid rheostat: Evolving concepts in cancer therapy. *Exp. Cell Res.* **333**, 195–200 (2015).
34. S. Rashad *et al*., Intracellular S1P levels dictate fate of different regions of the hippocampus following transient global cerebral ischemia. *Neuroscience* **384**, 188–202 (2018).
35. C. S. Petit *et al*., Inhibition of sphingolipid synthesis improves outcomes and survival in GARP mutant *wobbler* mice, a model of motor neuron degeneration. *Proc. Natl. Acad. Sci. U.S.A.* **117**, 10565–10574 (2020).
36. S. Furuya, J. Mitoma, A. Makino, Y. Hirabayashi, Ceramide and its interconvertible metabolite sphingosine function as indispensable lipid factors involved in survival and dendritic differentiation of cerebellar Purkinje cells. *J. Neurochem.* **71**, 366–377 (1998).
37. C. Ginkel *et al*., Ablation of neuronal ceramide synthase 1 in mice decreases ganglioside levels and expression of myelin-associated glycoprotein in oligodendrocytes. *J. Biol. Chem.* **287**, 41888–41902 (2012).
38. K. Wang *et al*., Alkaline ceramidase 3 deficiency results in Purkinje cell degeneration and cerebellar ataxia due to dyshomeostasis of sphingolipids in the brain. *PLoS Genet.* **11**, e1005591 (2015).
39. J. Matsuda *et al*., Mutation in saposin D domain of sphingolipid activator protein gene causes urinary system defects and cerebellar Purkinje cell degeneration with accumulation of hydroxy fatty acid-containing ceramide in mouse. *Hum. Mol. Genet.* **13**, 2709–2723 (2004).
40. J. Matsuda, A. Yoneshige, K. Suzuki, The function of sphingolipids in the nervous system: Lessons learnt from mouse models of specific sphingolipid activator protein deficiencies. *J. Neurochem.* **103** (suppl. 1), 32–38 (2007).
41. J. R. Sarna *et al*., Patterned Purkinje cell degeneration in mouse models of Niemann-Pick type C disease. *J. Comp. Neurol.* **456**, 279–291 (2003).
42. N. Hagen *et al*., Subcellular origin of sphingosine 1-phosphate is essential for its toxic effect in lyase-deficient neurons. *J. Biol. Chem.* **284**, 11346–11353 (2009).
43. N. Hagen, M. Hans, D. Hartmann, D. Swandulla, G. van Echten-Deckert, Sphingosine-1-phosphate links glycosphingolipid metabolism to neurodegeneration via a calpain-mediated mechanism. *Cell Death Differ.* **18**, 1356–1365 (2011).

44. L. Zhao *et al*., A deficiency of ceramide biosynthesis causes cerebellar purkinje cell neurodegeneration and lipofuscin accumulation. *PLoS Genet.* **7**, e1002063 (2011).
45. S. D. Spassieva *et al*., Ectopic expression of ceramide synthase 2 in neurons suppresses neurodegeneration induced by ceramide synthase 1 deficiency. *Proc. Natl. Acad. Sci. U.S.A.* **113**, 5928–5933 (2016).
46. H. B. Clark *et al*., Purkinje cell expression of a mutant allele of SCA1 in transgenic mice leads to disparate effects on motor behaviors, followed by a progressive cerebellar dysfunction and histological alterations. *J. Neurosci.* **17**, 7385–7395 (1997).
47. I. A. Klement *et al*., Ataxin-1 nuclear localization and aggregation: Role in polyglutamine-induced disease in SCA1 transgenic mice. *Cell* **95**, 41–53 (1998).
48. Y. Robitaille, L. Schut, S. J. Kish, Structural and immunocytochemical features of olivopontocerebellar atrophy caused by the spinocerebellar ataxia type 1 (SCA-1) mutation define a unique phenotype. *Acta Neuropathol.* **90**, 572–581 (1995).
49. S. Gilman, The spinocerebellar ataxias. *Clin. Neuropharmacol.* **23**, 296–303 (2000).
50. J. J. White *et al*., Region-specific preservation of Purkinje cell morphology and motor behavior in the ATXN1[82Q] mouse model of spinocerebellar ataxia 1. *Brain Pathol*, (2021).
51. N. Terada *et al*., Compartmentation of the mouse cerebellar cortex by sphingosine kinase. *J. Comp. Neurol.* **469**, 119–127 (2004).
52. E. N. Burright *et al*., SCA1 transgenic mice: A model for neurodegeneration caused by an expanded CAG trinucleotide repeat. *Cell* **82**, 937–948 (1995).
53. N. E. Sen *et al*., In human and mouse spino-cerebellar tissue, ataxin-2 expansion affects ceramide-sphingomyelin metabolism. *Int. J. Mol. Sci.* **20**, E5854 (2019).
54. M. L. Allende *et al*., Mice deficient in sphingosine kinase 1 are rendered lymphopenic by FTY720. *J. Biol. Chem.* **279**, 52487–52492 (2004).
55. K. Ishikawa *et al*., Calbindin-D 28k immunoreactivity in the cerebellum of spinocerebellar degeneration. *J. Neurol. Sci.* **129**, 179–185 (1995).
56. M. Cvetanovic, M. Ingram, H. Orr, P. Opal, Early activation of microglia and astrocytes in mouse models of spinocerebellar ataxia type 1. *Neuroscience* **289**, 289–299 (2015).
57. J. H. Kim, A. Lukowicz, W. Qu, A. Johnson, M. Cvetanovic, Astroglia contribute to the pathogenesis of spinocerebellar ataxia Type 1 (SCA1) in a biphasic, stage-of-disease specific manner. *Glia* **66**, 1972–1987 (2018).
58. A. Servadio *et al*., Expression analysis of the ataxin-1 protein in tissues from normal and spinocerebellar ataxia type 1 individuals. *Nat. Genet.* **10**, 94–98 (1995).
59. S. Rodriques *et al*., Slide-seq: A scalable technology for measuring genome-wide expression at high spatial resolution. *Science* **363**, 1463–1467 (2019).
60. Y. Sun *et al*., Combined saposin C and D deficiencies in mice lead to a neuronopathic phenotype, glucosylceramide and alpha-hydroxy ceramide accumulation, and altered prosaposin trafficking. *Hum. Mol. Genet.* **16**, 957–971 (2007).
61. H. E. Kong *et al*., Metabolic pathways modulate the neuronal toxicity associated with fragile X-associated tremor/ataxia syndrome. *Hum. Mol. Genet.* **28**, 980–991 (2019).
62. T. A. Couttas *et al*., Loss of the neuroprotective factor Sphingosine 1-phosphate early in Alzheimer's disease pathogenesis. *Acta Neuropathol. Commun.* **2**, 9 (2014).
63. Y. Xiong *et al*., Sphingosine kinases are not required for inflammatory responses in macrophages. *J. Biol. Chem.* **288**, 32563–32573 (2013).
64. O. Cuvillier *et al*., Suppression of ceramide-mediated programmed cell death by sphingosine-1-phosphate. *Nature* **381**, 800–803 (1996).
65. A. V. Alessenko, E. Albi, Exploring sphingolipid implications in neurodegeneration. *Front. Neurol.* **11**, 437 (2020).
66. H. K. Chen *et al*., Interaction of Akt-phosphorylated ataxin-1 with 14-3-3 mediates neurodegeneration in spinocerebellar ataxia type 1. *Cell* **113**, 457–468 (2003).
67. A. Lucaciu, R. Brunkhorst, J. M. Pfeilschifter, W. Pfeilschifter, J. Subburayalu, The S1P-S1PR axis in neurological disorders-insights into current and future therapeutic perspectives. *Cells* **9**, E1515 (2020).
68. M. Pitteri, R. Magliozzi, A. Bajrami, V. Camera, M. Calabrese, Potential neuroprotective effect of Fingolimod in multiple sclerosis and its association with clinical variables. *Expert Opin. Pharmacother.* **19**, 387–395 (2018).
69. M. Bigaud, D. Guerini, A. Billich, F. Bassilana, V. Brinkmann, Second generation S1P pathway modulators: Research strategies and clinical developments. *Biochim. Biophys. Acta* **1841**, 745–758 (2014).
70. A. Hoogendoorn *et al*., Variation in coronary atherosclerosis severity related to a distinct LDL (low-density lipoprotein) profile: Findings from a familial hypercholesterolemia pig model. *Arterioscler. Thromb. Vasc. Biol.* **39**, 2338–2352 (2019).
71. T. N. Luong, H. J. Carlisle, A. Southwell, P. H. Patterson, Assessment of motor balance and coordination in mice using the balance beam. *J. Vis. Exp.* **49**, 2376 (2011).
72. M. F. Vinueza Veloz *et al*., Cerebellar control of gait and interlimb coordination. *Brain Struct. Funct.* **220**, 3513–3536 (2015).